AIAA 93-3439
Application of a Two Camera Video Imaging System to Three-Dimensional Vortex Tracking in the 80- by 120-Foot Wind Tunnel

Larry A. Meyn
NASA Ames Research Center, Moffett Field, CA

Mark S. Bennett
Sterling Federal Systems, Inc., Palo Alto, CA

AIAA Applied Aerodynamics Conference

August 9-11, 1993 / Monterey, CA

APPLICATION OF A TWO CAMERA VIDEO IMAGING SYSTEM TO THREE-DIMENSIONAL VORTEX TRACKING IN THE 80- BY 120-FOOT WIND TUNNEL

Larry A. Meyn*
NASA Ames Research Center, Moffett Field, California 94035-1000

Mark S. Bennett†
Sterling Federal Systems, Inc., Moffett Field, California 94035

Abstract

A description is presented of two enhancements for a two-camera, video imaging system that increase the accuracy and efficiency of the system when applied to the determination of three-dimensional locations of points along a continuous line. These enhancements increase the utility of the system when extracting quantitative data from surface and off-body flow visualizations. The first enhancement utilizes epipolar geometry to resolve the stereo "correspondence" problem. This is the problem of determining, unambiguously, corresponding points in the stereo images of objects that do not have visible reference points. The second enhancement, is a method to automatically identify and trace the core of a vortex in a digital image. This is accomplished by means of an adaptive template matching algorithm. The system was used to determine the trajectory of a vortex generated by the Leading-Edge eXtension (LEX) of a full-scale F/A-18 aircraft tested in the NASA Ames 80- by 120-Foot Wind Tunnel. The system accuracy for resolving the vortex trajectories is estimated to be ± 2 inches over distance of 60 feet. Stereo images of some of the vortex trajectories are presented. The system was also used to determine the point where the LEX vortex "bursts". The vortex burst point locations are compared with those measured in small-scale tests and in flight and found to be in good agreement.

Nomenclature

b	- distance between cameras
c	- aerodynamic chord length
f	- focal length of a camera lens
h	- height dimension
O	- center of projection for a camera lens
R,**L**	- 3-D transformation matrices
r_{ij}, l_{ij}	- matrix coefficients
s	- length dimension
x,y,z	- orthogonal position coordinates
θ	- angle dimension

subscripts

i,j	- matrix coefficient indices
l	- left camera coordinate system
r	- right camera coordinate system
w	- world camera coordinate system

superscripts

'	- denotes image plane coordinates

Introduction

A low-cost, video imaging system for three-dimensional, stereo ranging has been developed for use in large-scale wind tunnel tests.[1,2] Potential applications include vortex tracking, tracing of surface and off-body streamlines, and measurement of model positions and deflections. This paper first describes the development two enhancements that increase the accuracy and efficiency of the system when applied to the determination of three-dimensional locations of points along a continuous line. Some results are then presented of three-dimensional vortex trajectory measurements obtained during tests of a full-scale F/A-18 aircraft in the 80- by 120-Foot Wind Tunnel.[3]

The first enhancement to the stereo ranging system was a method of resolving the stereo "correspondence" problem for objects like flow field streamlines that are made visible by common flow visualization techniques. The stereo ranging system determines the three-dimensional location of point from the two-dimensional coordinates of the image of that point on each camera's image plane. The "correspondence" problem in stereo ranging, is to identify points in each image that correspond a single point on the object being measured. The initial application of the system, which was to measure the angle-of-attack of parafoils tested in the 80- by 120-Foot Wind Tunnel[4], used visual markers sewn on to the parafoils to identify corresponding point locations in the two stereo images. However, when tracking the path of a smoke-enhanced vortex or streamline, no such marking system is readily available. Although a laser light sheet could be used to mark locations on the vortex, the number of points would be limited and the overall complexity of the system would be increased. Instead, the method chosen to resolve the stereo correspondence problem for vortices and streamlines utilizes geometric constraints that are imposed by epipolar geometry inherent in stereo systems.

The second enhancement, is a method to automatically identify and trace the core of a vortex in a digitized image. To method uses template matching to identify and locate cross-sections of the vortex image.

---

* Aerospace Engineer. Member AIAA.

† Professional Staff.

Template matches are made using digital cross-correlation. A single template cannot be used, since the vortex broadens as it moves downstream and the template must broaden accordingly. Therefore, the method developed utilizes an adaptive template.

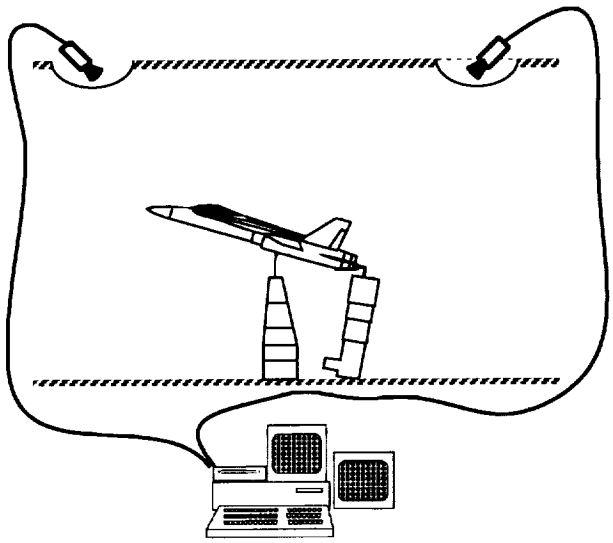

Figure 1 Schematic of the Stereo Ranging System Configuration for the F/A-18.

These enhancements to the stereo ranging system first used to track vortices generated by the leading edge extension (LEX) of an full-scale F/A-18 at various angles of attack. Two video cameras were arranged as shown in Figure 1. One is mounted in the ceiling upstream of the F/A-18 aircraft and the other is mounted in the ceiling downstream of the aircraft. Smoke is injected into the flow near the apex of the LEX to make the LEX vortex visible. The LEX vortex is also often visible when humidity and temperature conditions are such that water vapor condenses within the vortex. Images from each camera, such as those shown in Figure 2, are captured and displayed on computer monitors. The images are then processed to determine the two-dimensional track of the vortex in each image. The two vortex tracks are then used to reconstruct the three-dimensional trajectory of the vortex.

Figure 2 View of the F/A-18 from the left camera.

Theory

Stereo Ranging

Stereo range finding is a three-dimensional procedure that locates a point in space by triangulation. Figure 3 shows a simple, two-dimensional representation of the geometric relationships involved. The camera images are modeled as "line-of-sight" projections of scenes onto image planes (i.e. video screens). The image planes are placed at a distance, f_r and f_l in front of their respective focal points, O_r and O_l. Each camera has a coordinate system centered on it's focal point and is oriented with the z-axis perpendicular to the image plane.

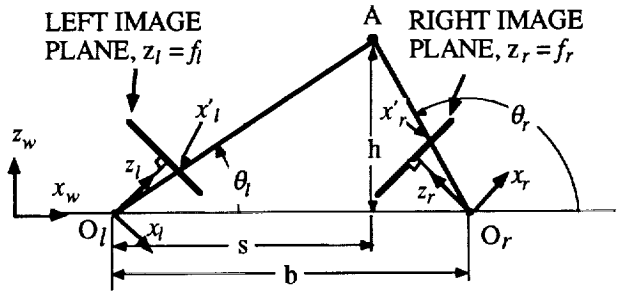

Figure 3 Two-dimensional triangulation.

In this figure, the goal is to locate Point A using its images projected onto the left and right image planes. Point A is at location (x_W, y_W, z_W) in the spatial or world coordinate system. Point A projects onto the left and right image planes at locations (x'_l, f_l) and (x'_r, f_r) in the left and right camera coordinate systems, respectively. If the position and orientation of each camera is known, then the angles θ_l and θ_r can be determined from x'_l and x'_r. Knowledge of the two angles (θ_l and θ_r) and the distance between the two focal points b, makes it possible to determine the position of Point A by use of trigonometric relationships.

While trigonometric relationships are useful in understanding how a stereo ranging system works, they are impractical to implement for generalized three-dimensional system configurations because the camera locations, camera geometries, and camera orientations cannot be determined accurately enough for the desired resolution. Instead, a generalized matrix model is used, where each point in space is represented by a location vector for a particular coordinate system. Thus, to calibrate a camera, a location vector is converted from the external "world" coordinate system to the camera coordinate system by multiplying it by a transformation matrix. The relationship is expressed below for the *right* camera member of the stereo pair.

$$
\begin{aligned}
r_{11}x_w + r_{12}y_w + r_{13}z_w + r_{14} &= x_r \\
r_{21}x_w + r_{22}y_w + r_{23}z_w + r_{24} &= y_r \\
r_{31}x_w + r_{32}y_w + r_{33}z_w + r_{34} &= z_r
\end{aligned} \tag{1}
$$

The coefficients, r_{ij}, are the calibration coefficients for the *right* camera; the vector, (x_w, y_w, z_w), represents a point in the external "world" coordinate system; and the vector, (x_r, y_r, z_r), represents the same point in the *right* camera coordinate system. A similar equation set is used for the *left* camera.

The camera image is a projection of a three-dimensional image onto a two-dimensional image plane, i.e., a video screen. Only the intersection of the three-dimensional image vector, (x_r, y_r, z_r), with the image plane is known. Since all points on the image plane have a z-value equal to the focal length, f_r, the vector (x'_r, y'_r) is used to describe points on the image plane. By use of similar triangles, the variables x'_r and y'_r are related to the three-dimensional camera coordinates by the following equations.

$$\frac{x'_r}{f_r} = \frac{x_r}{z_r} \tag{2a}$$

$$\frac{y'_r}{f_r} = \frac{y_r}{z_r} \tag{2b}$$

If a point in the right image, (x'_r, y'_r), and the corresponding point in the left image, (x'_l, y'_l) are known, the world coordinate vector, (x_w, y_w, z_w), can be recovered using the following relationship.

$$(x'_r r_{31} - r_{11})x_w + (x'_r r_{32} - r_{12})y_w + (x'_r r_{33} - r_{13})z_w = r_{14} - x'_r \tag{3a}$$

$$(y'_r r_{31} - r_{21})x_w + (y'_r r_{32} - r_{22})y_w + (y'_r r_{33} - r_{23})z_w = r_{24} - y'_r \tag{3b}$$

$$(x'_l l_{31} - l_{11})x_w + (x'_l l_{32} - l_{12})y_w + (x'_l l_{33} - l_{13})z_w = l_{14} - x'_l \tag{3c}$$

$$(y'_l l_{31} - l_{21})x_w + (y'_l l_{32} - l_{22})y_w + (y'_l l_{33} - l_{23})z_w = l_{24} - y'_l \tag{3d}$$

Point Correspondence

Equation set (3) assumes that the corresponding screen location of the point in object space is known in each camera view. When finding the angle of attack of parafoils[1,4], markers were sewn on the parafoils to make the determination. However, in the case of vortex tracking, a smoke filled vortex essentially presents a continuous line in both images, which makes it difficult to visually identify corresponding points. This is where epipolar geometry is used.

Figure 4 illustrates the basic elements of epipolar geometry. An epipolar plane is defined by a point on the vortex path and the two camera focal points. The intersection of an epipolar plane with the image planes is a pair of epipolar lines, along which the image of the point on the vortex must lie. The same epipolar plane can also be defined by a point on the left camera image and the two camera focal points. By choosing a point on the vortex track in the one image, an epipolar line can be computed for the other image. The intersection of the epipolar line with the vortex track in the second image provides the location of the point corresponding to the point chosen in the first image.

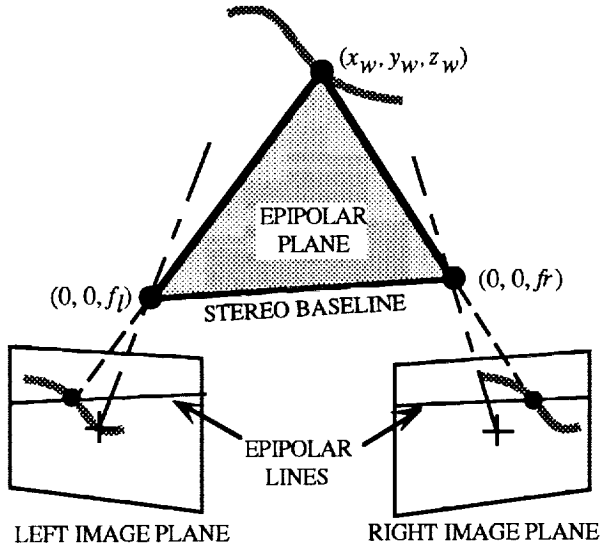

Figure 4 Epipolar Geometry.

The equation for epipolar lines is derived as follows. Equation set (3) is rearranged to form the following homogeneous matrix equation.

$$\begin{bmatrix} (x'_r r_{31} - r_{11}) & (x'_r r_{32} - r_{12}) & (x'_r r_{33} - r_{13}) & (x'_r - r_{14}) \\ (y'_r r_{31} - r_{21}) & (y'_r r_{32} - r_{22}) & (y'_r r_{33} - r_{23}) & (y'_r - r_{24}) \\ (x'_l l_{31} - l_{11}) & (x'_l l_{32} - l_{12}) & (x'_l l_{33} - l_{13}) & (x'_l - l_{14}) \\ (y'_l l_{31} - l_{21}) & (y'_l l_{32} - l_{22}) & (y'_l l_{33} - l_{23}) & (y'_l - l_{24}) \end{bmatrix} \begin{bmatrix} x_w \\ y_w \\ z_w \\ 1 \end{bmatrix} = \begin{bmatrix} 0 \\ 0 \\ 0 \\ 0 \end{bmatrix} \tag{4}$$

Equation (4) has a solution when the determinant of the 4x4 matrix is zero. Following the method described by Schalkoff[4], the determinant can be expanded, set equal to zero, and reorganized to produce the following bilinear equation:

$$
\begin{aligned}
&m_1 x'_r x'_l + m_2 x'_r y'_l + m_3 y'_r x'_l + \\
&m_4 y'_r y'_l + m_5 x'_r + m_6 x'_l + \\
&\qquad m_7 y'_r + m_8 y'_l + m_9 = 0
\end{aligned} \tag{5}
$$

In equation (5), the coefficients, m_i, consist of combinations of the coefficients of the two transformation matrices. As an example of how equation (5) is used, assume a point on the vortex is chosen in the left image. When the coordinates for this point are entered into equation (5), the resultant equation describes an epipolar line in the right image. The intersection of the epipolar line with the vortex track in the right image is the point

corresponding the chosen point in the left image. The coordinates of the two image points are then used in equation set (3) to determine the three-dimensional location of the actual point on the vortex.

Vortex Image Enhancement

When a pair of stereo images for vortex tracking are recorded, the first step is to determine the coordinates for the vortex track in each image. To simplify the process, a region of interest surrounding the vortex in each image is selected, such as is shown in Figure 5. From these regions, reference images of the aircraft without a visible vortex are subtracted. This helps isolate the vortex, but a few aircraft features still remain due to differences in lighting and model deflections when the reference images were recorded. Following image subtraction, a vortex can often be isolated by applying a threshold to the image. This is accomplished by making all pixels with a brightness value above a certain level white and all the remaining pixels are made black. Unfortunately, with the F/A-18 LEX vortex images, it was not possible to isolate the image of the LEX vortex from the image of the white paint along the LEX edge using the thresholding method. To isolate the vortex in this situation requires a more sophisticated technique.

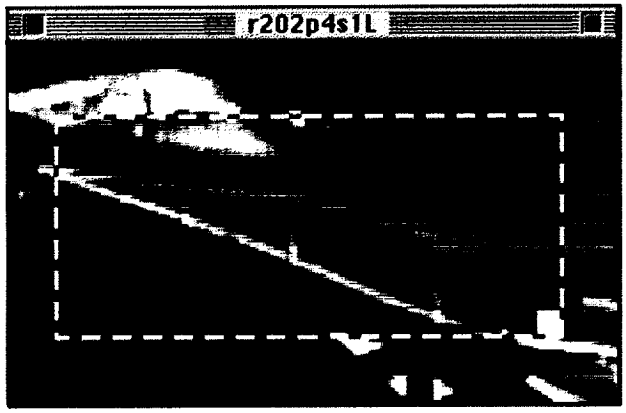

Figure 5(a) The vortex in the left camera image.

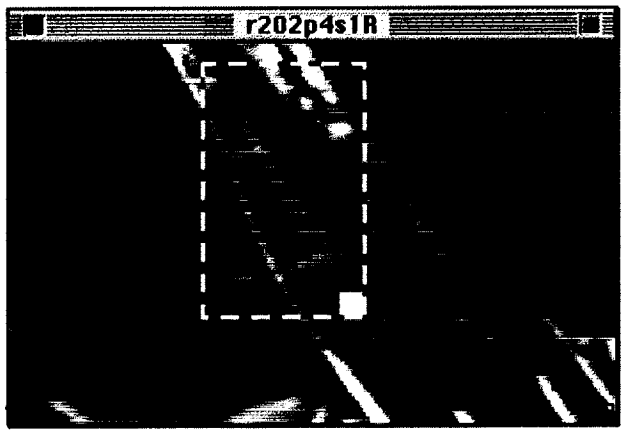

Figure 5(b) The vortex in the right camera image.

In order to determine which pixels belong to the core of the vortex, the assumption is made that the densest smoke digitizes and corresponds to the brightest pixels. Figure 6 shows pixel values versus pixel location for a cross-sectional "slice" through the vortex in the image. This can be thought of as the local vortex "signature" and the peak is assumed to be the core or center of the vortex. To track the vortex, the selected region of interest is divided into columns (or rows). The location of the vortex core in each column is determined from a cross-correlation of the pixel value distribution in the column with a template of the vortex signature. This method is very robust, and it easily picks out the vortex core even when the pixel value distribution contains some aircraft remnants, such as white paint on the LEX as shown in Figure 7.

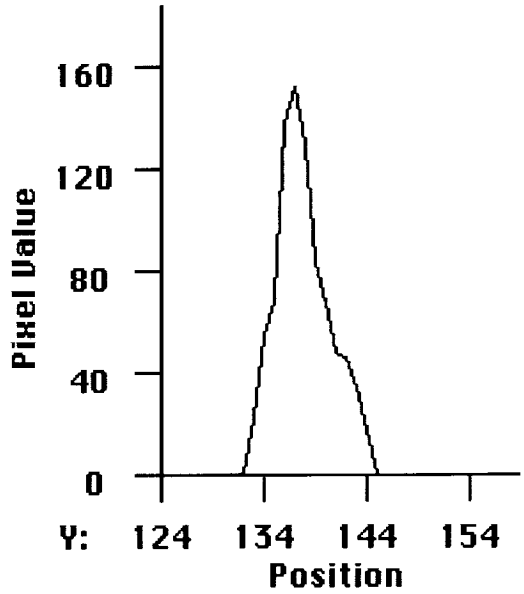

Figure 6 A vortex signature template.

However, a single vortex template cannot be used for the entire length of the vortex, because, as the point in question moves downstream from the vortex origin, the smoke diffuses and the vortex signature broadens. Recognizing that this is a gradual change, a convenient means by which a local template may be provided is to use the pixel distribution of the previous column. Once a template match is found and the peak location determined, the template is replaced by the current cross-section and this new template is used on the next column. Thus, as the vortex signature changes shape, the template adapts. For the very first iteration, however, the user has to provide initial templates for the left and right images. This is done by identifying a representative line of pixels across the vortex near the origin. The starting templates can be saved, and a single pair of starting templates can be used for several similar images.

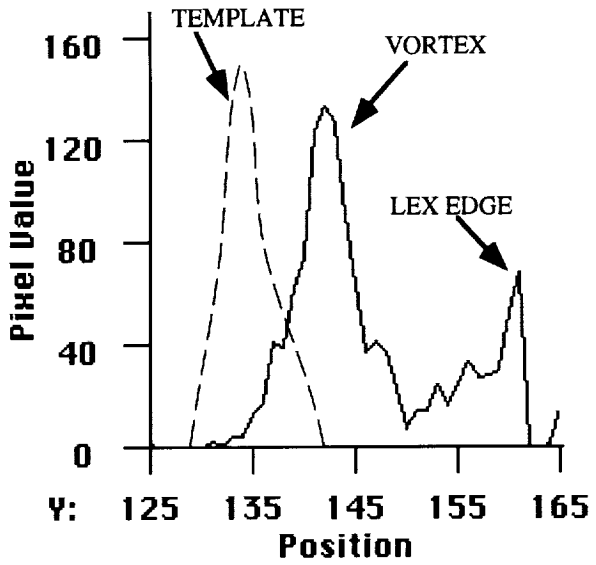

Figure 7 A vortex signature template and an image cross-section containing the vortex and the LEX edge.

The correlation method comes from reference 6. The row (or column) of pixels containing image data is represented by the discrete function, g_k, and the template pixels by the discrete function, h_k. The correlation function, $Corr(g,h)_j$, is found by taking the Fourier transforms of g_k and h_k, and multiplying one by the complex conjugate of the other as is shown in the following equation.

$$Corr(g,h)_j = G_k H_k^* \qquad (6)$$

In equation (6) G_k and H_k are the discrete Fourier transforms of g_k and h_k and the subscript, j, denotes the lag between the two functions. If the maximum of the cross-correlation occurs at $j = 0$, then the functions coincide. If the maximum occurs at a lag other than zero, then the lag indicates the distance in pixels between the peak in the template and the peak in the image data. In this way the position of the vortex core can be easily identified. Figure 8 shows the results of the correlation matching algorithm on a typical vortex image, wherein the algorithm was able to ignore the remnant image of the LEX edge which intersects the vortex trail.

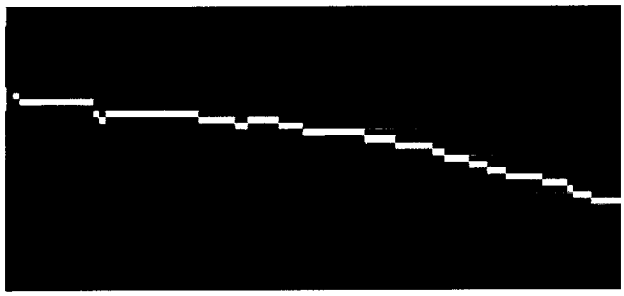

Figure 8 The vortex track determined by the template matching algorithm overlaid on the source image of the vortex and LEX edge.

To represent the vortex as a continuous function, a least squares curve fit is made to the pixels identified as lying along the image of vortex core. After a continuous function has been determined for both the left and right vortex images, then one image is chosen as the reference image from which the epipolar lines are determined for the other image. The intersection of the epipolar lines with the function describing the image of the vortex core yields a list of corresponding points from which the three-dimensional vortex track is determined.

Results

In order to obtain the flow visualization images of the F/A-18 vortex trail, the wind tunnel was operated at a speed of 92 ft/sec (10 psf dynamic pressure). At angles-of-attack tested, the F/A-18 LEX generates a very strong vortex. At some distance downstream of the origin, the vortex undergoes what is referred to as "vortex burst". The point where the smoke-enhanced suddenly expands is the location of the vortex burst. This point is not steady, even when the aircraft maintains a fixed angle-of-attack. Instead, the burst point tends to moves fore and aft over a short range. As the aircraft increases angle-of-attack from 18 to 50 degrees, the burst point moves forward. Figure 9 shows a side view of the LEX vortex path up to the burst point for angles-of-attack of 25°, 30°, 35°, and 40°. The length of the vortex is shown to decrease with angle-of-attack. The three-dimensional trajectories for these same angles-of-attack are presented as a stereo image pair in Figure 10. The burst point as a function of angle-of-attack for the full-scale F/A-18 test is shown in Fig 11 along with burst point data from flight tests[7], 11%-scale wind-tunnel tests[8], 6%-scale wind-tunnel tests[9] and a 2-% scale water-tunnel test[10]. As can be seen, the vortex burst locations for all of these tests are in good agreement.

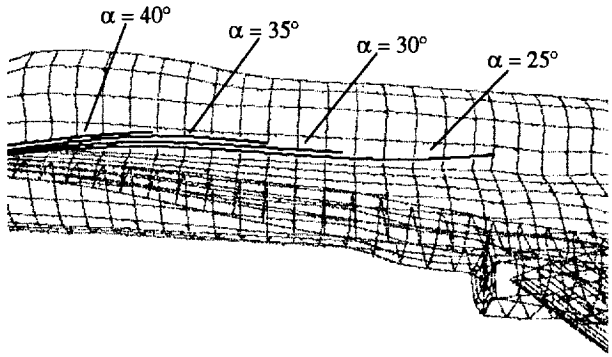

Figure 9 Vortex trajectories for several angles-of-attack superimposed on a wire-frame model of the aircraft.

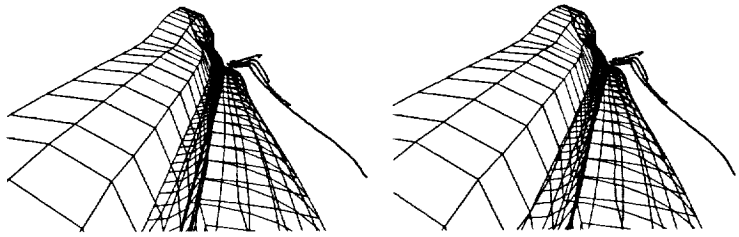

Figure 10 A stereo pair showing vortex trajectories at four angles-of-attack superimposed on a wire-frame model of the aircraft. The view is from the above, right, rear position.

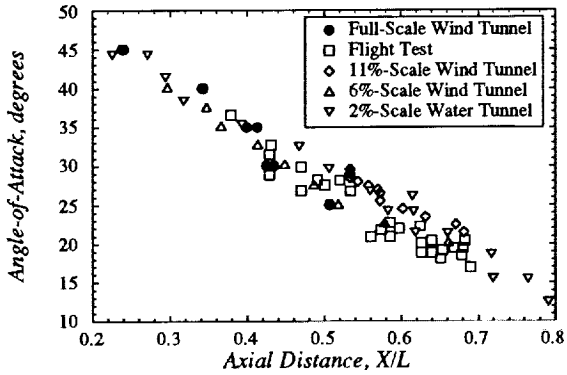

Figure 11 F/A-18 vortex burst location as a function of angle-of-attack for several model scales.

Conclusion

This paper described two enhancements to a two-camera video imaging system that improved the accuracy and efficiency the system when used to track the three-dimensional vortices generated by the LEX of a full-scale F/A-18 aircraft. Two steps were involved in the process. The first enhancement was to use epipolar geometry to identify corresponding points along the vortex in both camera images. The second enhancement was the development and implementation of a fast and robust algorithm to locate a vortex core in digital image that contains misleading image fragments.

Using stereo image data from a full-scale F/A-18 wind tunnel test, the three-dimensional vortex trajectories computed by the system are estimated to be within ±2 inches over a range of 60 feet. Burst point locations determined by the system were shown to agree very well with burst point locations determined in small-scale tests and in flight.

References

1 Meyn, L. and Bennett, M.: "A Two Camera Video Imaging System With Application to Parafoil Angle-of-Attack Measurements", AIAA Paper 91-0673, AIAA Aerospace Sciences Meeting, January 1991.

2 Bennett, M.S.: "The Stereo Ranging Program (SRP): Programmer's Manual and User's Guide for the ARS II Version", Sterling TN-90-2000-205-102, Sterling Federal Systems, Palo Alto, CA, May 1990.

3 Meyn, L.A., Lanser, W.R., and James, K.D.: "A Two Camera Video Imaging System With Application to Parafoil Angle-of-Attack Measurements", AIAA Paper 91-0673, AIAA Aerospace Sciences Meeting, January 1991.

4 Ross, J.C. and Olson, M.E.: "Experience with Scale Effects in Non-Airplane Wind Tunnel Testing", AIAA Paper 90-1822, AIAA Aerospace Engineering Conference and Show, February 1990.

5 Schalkoff, R.J., Digital Image Processing and Computer Vision, John Wiley & Sons, New York, 1989.

6 Press, H.P., Flannery, B.P., Teukolsky, S.A., and Vetterling, W.T., Numerical Recipes: The Art of Scientific Computing, Cambridge University Press, Cambridge, 1986.

7 Fisher, D.F. and Meyer, R.R., Jr.: "Flow Visualization techniques for Flight research", NASA TM 100455, 1988.

8 Martin, C.A., Glaister, M.K., MacLaren, L.D., Meyn, L.A., and Ross, J.: "F/A-18 1/9th Scale Model Tail Buffet Measurements", Flight Mechanics Report 188, Aeronautical Research Laboratory, Melbourne Australia, June 1991.

9 Erickson, G.E.: "Wind Tunnel Investigation of Vortex Flows on F/A-18 Configuration at Subsonic Through Transonic Speeds", NASA Technical Paper 3111, December 1991.

10 Thompson, D.H.: "Water Tunnel Flow Visualization of Vortex Breakdown Over the F/A-18", Flight Mechanics Report 179, Aeronautical Research Laboratory, Melbourne Australia, 1990.